SUPPLEMENTAL INFORMATION

Figure S1

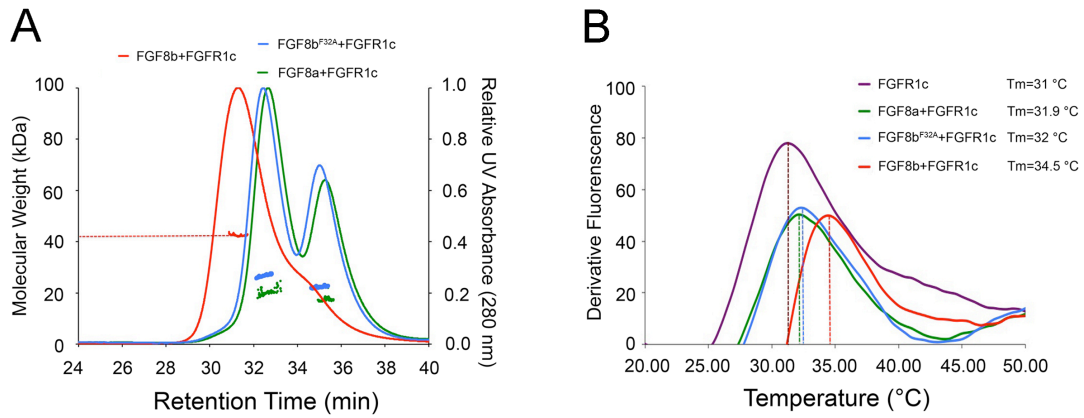

Figure S1. The differences in the stabilization of FGF-FGFR complex induced by FGF8 isoforms in the absence of HS. Related to Figure 1.

(A) SEC-MALLS analysis of the binding affinity of FGFR1c with FGF8a, FGF8b or FGF8b^{F32A}, respectively. Each ligand was mixed with the FGFR1c ligand-binding domain at a molar ratio of 1.2:1, and the mixtures were injected into an TSK-Gel® SuperSW3000 gel filtration column and eluted with phosphate-buffered saline buffer (pH7.4). The 280 nm UV absorbance traces for the FGF8a-FGFR1c, FGF8b-FGFR1c, and FGF8b^{F32A}-FGFR1c complexes are colored green, red and blue, respectively. A second line below each protein complex peak denotes the peak area selected for molecular weight calculation. **(B)** Thermal stability of FGFR1c ectodomain in the presence of different ligands (FGF8a/FGF8b/FGF8b^{F32A}). The FGFR1c stability was analyzed by a fluorescence-based thermal shift assay as described in 'Materials and Methods' section, in the absence (purple curve) or in the presence of 50 mM FGF8a/FGF8b/FGF8b^{F32A} (green, blue and red curves, respectively). The melting temperature (Tm) is obtained from the first derivatives of the fluorescence signal from the melting curves of FGFR1c alone or in the presence of different ligands, calculated with StepOne software v2.2.

Figure S2

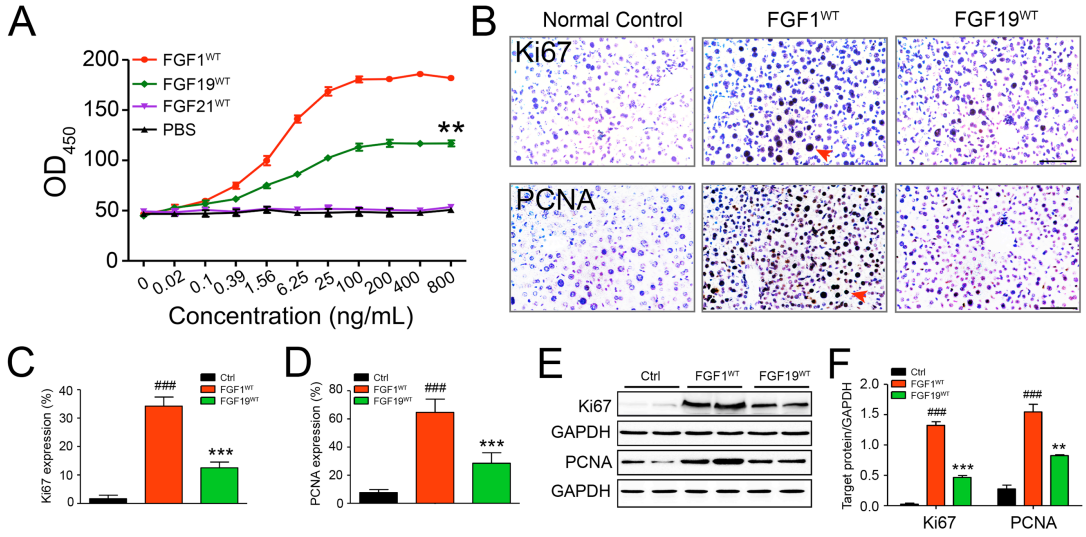

Figure S2. The comparison of the mitogenic potentials of FGF1^{WT} and FGF19^{WT} *in vitro* and *in vivo*. Related to Figures 2 and 5.

(A) The comparison of the mitogenic potentials of FGF1^{WT}, FGF19^{WT} and FGF21^{WT} in H4IIE cells using an MTT-based assay. Data from three independent measurements are presented as mean +/- SEM. **p<0.01 vs FGF1^{WT}. **(B)** Microscopic images of mouse liver tissue sections stained for proliferating cell nuclear antigen (PCNA) and Ki67. Liver tissue was isolated from normal C57BL/6J mice intraperitoneally treated with FGF1^{WT} or FGF1$^{\triangle HBS}$ (2.0 mg/kg body weight) once daily for twenty days. Note the increased number of PCNA- and Ki67-positive cell nuclei in liver tissue from FGF1^{WT}-treated mice compared with liver tissue from FGF19^{WT} -treated mice. Data are representative of 6 mice from each group. Scale bar, 50 μm. **(C&D)** The quantitative assessment of Ki67 and PCNA-positive cells in pane B. **(E&F)** Immunoblot analysis (E) and its corresponding densitometric analysis (F) for PCNA and Ki67 protein expression in liver tissues from mice intraperitoneally treated with 2.0 mg/kg body weight FGF1^{WT} or FGF19^{WT} every day for twenty days. Data in panels C, E, F are presented as mean +/- SEM (n=6). ###p<0.001 vs normal control; **p<0.01, ***p<0.001 vs FGF1 treatment group. This figure is related to Figures 2 and 5.

Figure S3

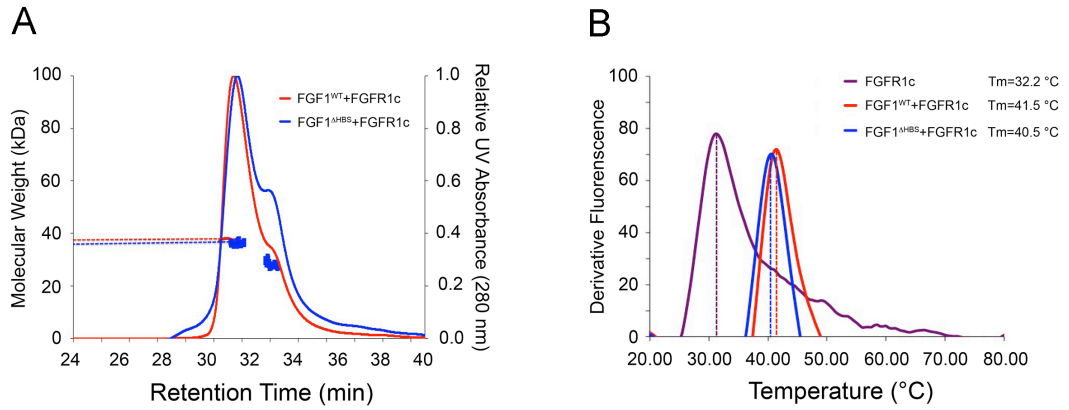

Figure S3. The differences in the stabilization of FGF-FGFR complex induced by wild-type FGF1 and FGF1$^{\triangle HBS}$. Related to Figure 3.

(A) SEC-MALLS analysis of the binding affinity of FGFR1c with wild-type FGF1 and FGF1$^{\triangle HBS}$, respectively. FGF1^{WT} or FGF1$^{\triangle HBS}$ (MW=17.4 kDa) was mixed with the FGFR1c ligand-binding domain (MW=25.4 kDa) at a molar ratio of 1.2:1, and the mixtures were injected into an TSK-Gel® SuperSW3000 gel filtration column and eluted with phosphate-buffered saline buffer (pH7.4). The elution profile of a mixture of FGF1^{WT} with the FGFR1c ligand-binding domain alone served as a control. The 280 nm UV absorbance traces for the FGF1^{WT}-FGFR1c and FGF1$^{\triangle HBS}$-FGFR1c complexes are colored red and blue, respectively. A second line below each protein complex peak denotes the peak area selected for molecular weight calculation. **(B)** Thermal stability of FGF1^{WT}-FGFR1c (red curve) and FGF1$^{\triangle HBS}$-FGFR1c (blue curve) complexes by measuring their unfolding temperatures (Tm) using a fluorescence dye-based thermal shift assay.

Figure S4

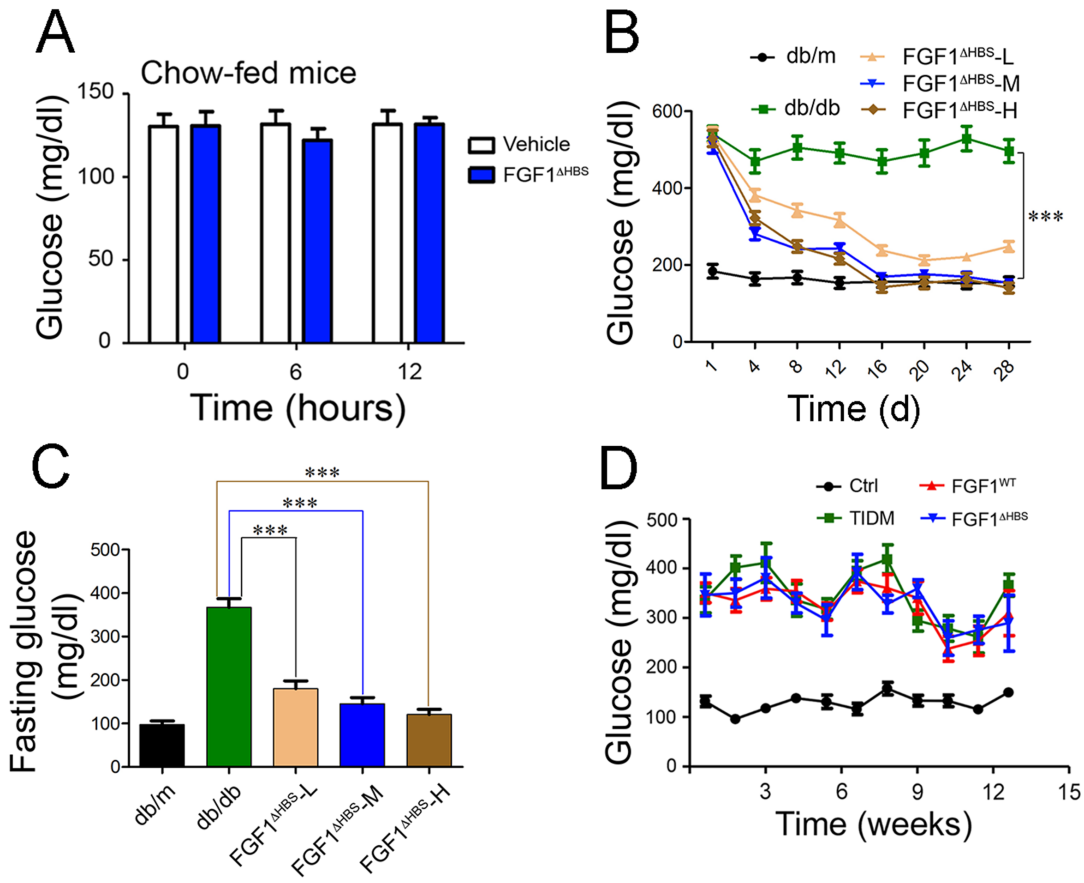

Figure S4. Effects of FGF1^{WT} and FGF1$^{\Delta HBS}$ on glucose levels in experimental mice. Related to Figure 6.

(A) Effect of a single IP injection of FGF1$^{\triangle HBS}$ (0.5 mg/kg body weight) on fed-state blood glucose levels in chow-fed mice. Blood glucose levels in chow-fed mice injected with vehicle (PBS) served as a control. Data are presented as mean +/- SEM (n=7). **(B)** Dose response curve represented as fed-state blood glucose levels over the course of a 28-day chronic treatment of *db/db* mice with FGF1$^{\triangle HBS}$. The doses used were Low: L (0.2mg/kg body weight), Medium: M (0.5mg/kg body weight) and High: H (1.0mg/kg body weight). Data are presented as mean +/- SEM (n=9). ***p<0.001 vs *db/db*. **(C)** Evaluation of fasting glucose levels in db/db mice following the 28-day chronic treatment with FGF1$^{\triangle HBS}$ at all 3 doses administered (L, M and H). **(D)** Fed-state blood glucose levels over the course of a 3-month treatment of STZ-induced type 1 diabetic mice with FGF1^{WT} or FGF1$^{\triangle HBS}$ (0.5 mg/kg body weight). Data are presented as mean +/- SEM (n=8).

Figure S5

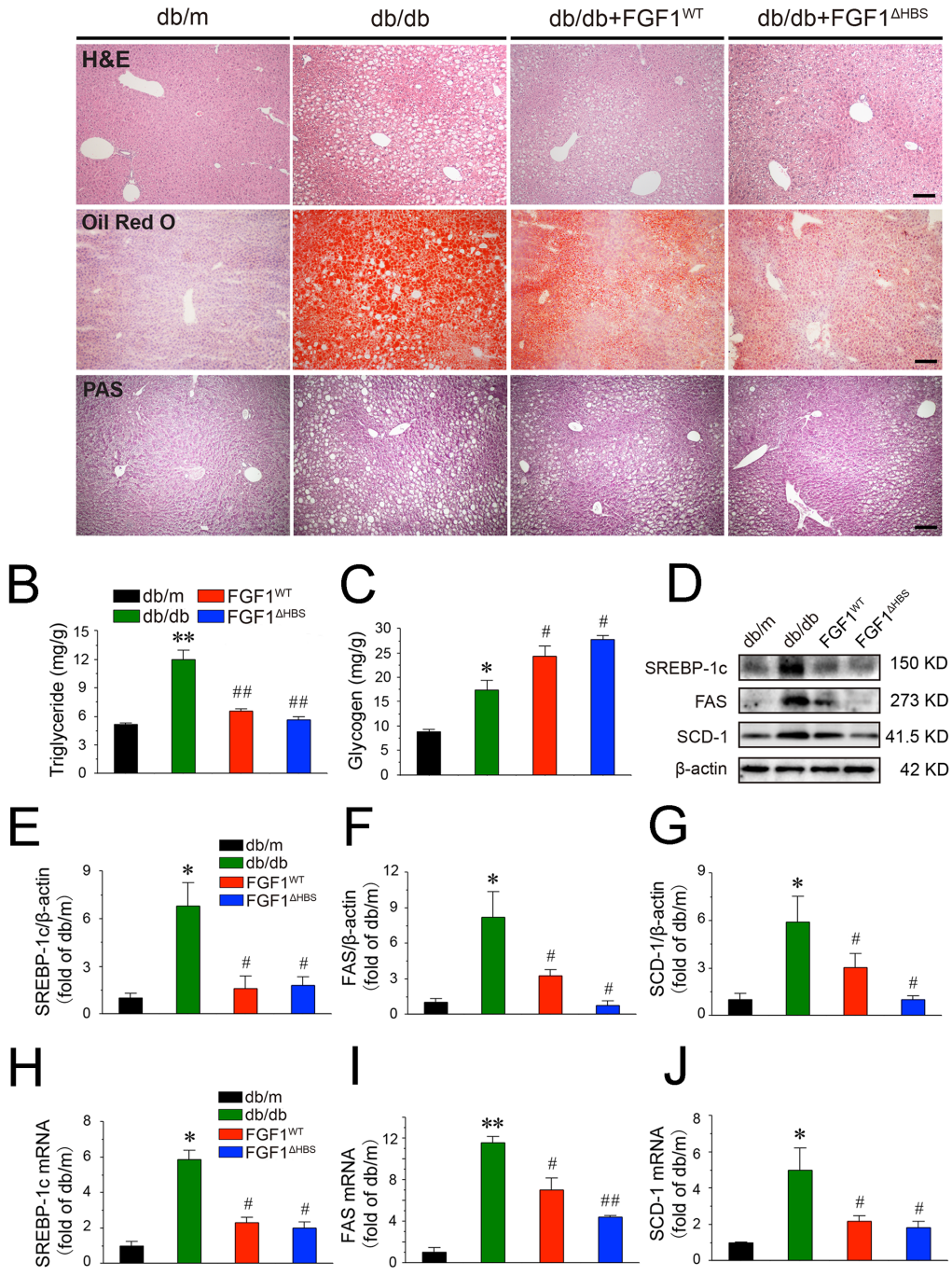

Figure S5. Chronic effects of FGF1^{WT} and FGF1$^{\triangle HBS}$ on hepatic lipid and glucose metabolism in *db/db* mice. Related to Figure 6.

(A) Microscopic images of murine liver tissue sections stained with haematoxylin and eosin (H&E), Oil Red O, or periodic acid–Schiff reagent (PAS). Liver tissue was isolated from *db/db* mice treated with FGF1^{WT} or FGF1$^{\triangle HBS}$ for 28 days (0.5 mg/kg body weight). Liver tissues from untreated *db/db* mice and their littermates (*db/m*) served as controls. Red dots in the Oil Red O stained tissue sections indicate microvesicular and macrovesicular steatosis, and magenta regions in the PAS stained tissue

sections represent glycogen. Data are representative of 7 mice from each group. Scale bar, 500 μm. **(B&C)** Triglyceride content (B) and Glycogen content (C) in liver tissue from *db/db* mice treated with $FGF1^{WT}$ or $FGF1^{\triangle HBS}$ for 28 days (0.5 mg/kg body weight). Liver tissues from untreated *db/db* mice and their littermates (*db/m*) served as controls. Data are presented as mean +/- SEM (n=7). *p<0.05 vs *db/m*; #p<0.05 vs *db/db*. **(D-J)** Immunoblot analysis for liver protein expression (D-G) and real-time quantitative PCR analysis for liver mRNA expression (H-J) of enzymes or transcription factors (i.e. SREBP-1a [E and H], FAS [F and I], SCD-1[G and J]) involved in lipogenesis and triglyceride synthesis. Total cellular protein or RNA was isolated from liver tissue of *db/db* mice treated with $FGF1^{WT}$ or $FGF1^{\triangle HBS}$ for 28 days (0.5 mg/kg body weight). Liver tissues from untreated *db/db* mice and their littermates (*db/m*) served as controls. Protein and mRNA levels were normalized to *db/m* control values. Data are presented as mean +/- SEM (n=7). *p<0.05, **p<0.01 vs *db/m*; #p<0.05, ##p<0.01 vs *db/db*.

Figure S6

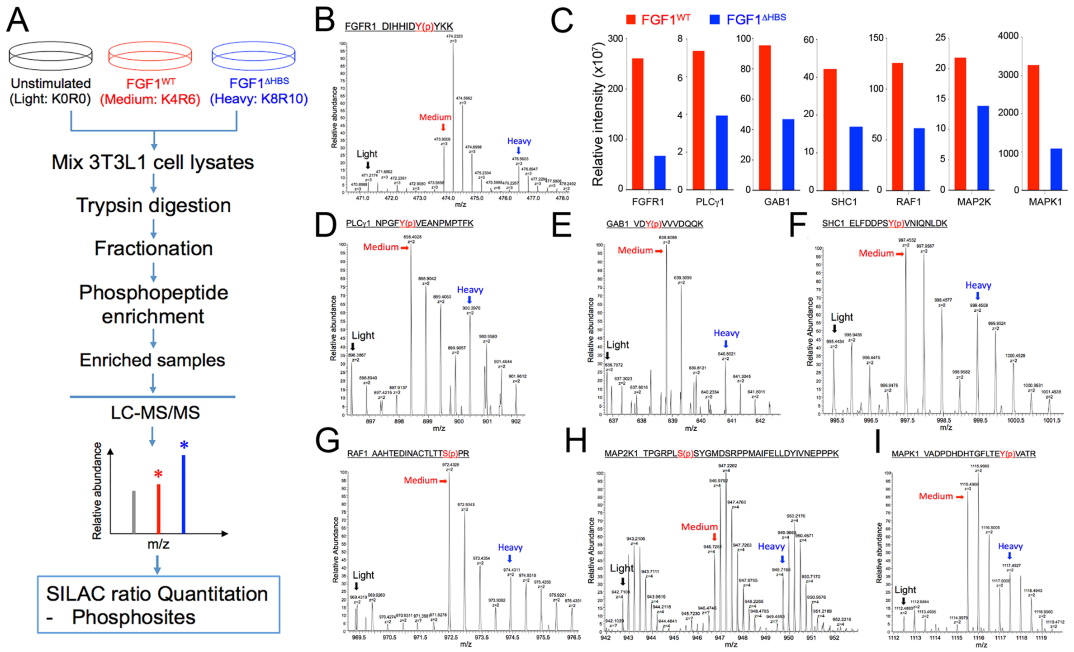

Figure S6. Phosphopeptide quantitation using SILAC. Related to Figures 3, 4 and 7. **(A)** Flow chart showing the process of cell labeling by SILAC, sample preparation and mass spectrometry for phosphopeptide analysis. **(B, D-I)** SILAC pairs are shown for different phosphopeptides including, FGFR1-DIHHIDY (p) YKK (B), PLCγ1- NPGFY (p) VEANPMPTFK (D), GAB1- VDY (p) VVVDQQK (E), SHC1- ELFDDPSY (p) VNIQNLDK (F), Raf1-AAHTEDINACTLTTS (p) PR (G), MAP2K1-TPGRPLS (p) SYGMDSRPPMAIFELLDYIVNEPPPK (H), MAPK1-VADPDHDHTGFLTEY (p) VATR (I). The lower-mass peak clusters (black arrow showing the monoisotopic peak) are from light Arg/Lys peptides of unstimulated cells, and the medium-mass peak clusters (red arrow) are from medium Arg/Lys peptides of $FGF1^{WT}$ stimulated cells, while the higher-mass peak clusters (blue arrow) are from heavy Arg/Lys peptides of $FGF1^{\Delta HBS}$ stimulated cells. For example, in Figure B, peptide ions shown are triply charged and the m/z difference between the light and medium peaks or the medium and heavy peaks is 2.67 (mass difference is 8 Da), while in Figure I, the peptide ions shown are doubly charged and the m/z difference between the light and medium peaks is 3 (mass difference is 6 Da), and between the medium and heavy peaks is 2 (mass difference is 4 Da). **(C)** Ratios were determined by comparing the relative intensities from medium or heavy versions of each phosphorylated peptide.

Figure S7

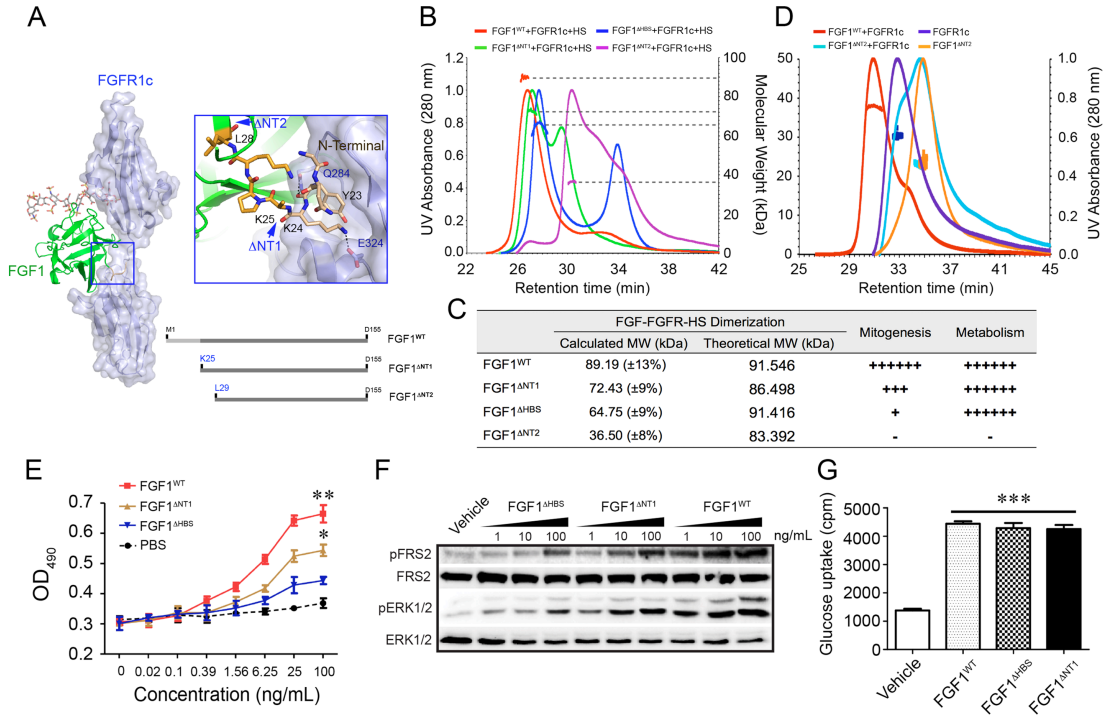

	FGF-FGFR-HS Dimerization		Mitogenesis	Metabolism
	Calculated MW (kDa)	Theoretical MW (kDa)		
$FGF1^{WT}$	89.19 (±13%)	91.546	++++++	++++++
$FGF1^{\Delta NT1}$	72.43 (±9%)	86.498	+++	++++++
$FGF1^{\Delta HBS}$	64.75 (±9%)	91.416	+	++++++
$FGF1^{\Delta NT2}$	36.50 (±8%)	83.392	-	-

Figure S7. The differences in the stabilization of 2:2 FGF-FGFR dimers and the cellular response induced by $FGF1^{WT}$ and its variants. Related to Figures 3, 4 and 7.

(A) Cartoon representation of the crystal structure of the FGF1-FGFR1c complex (PDB ID: 1EVT) with a modeled HS oligosaccharide (shown as sticks) based on the crystal structure of the FGF2-FGFR1c-HS complex (PDB ID: 1FQ9). FGF1 and FGFR1c are colored green and light blue, respectively, and the HS oligosaccharide is colored grey. The N-terminal region of FGF1 is shown as sticks, and black dashed lines denote the hydrogen bonds between FGF1 and FGFR1c. Truncations at residues K24 and L28 of FGF1 that generate $FGF1^{\triangle NT1}$, and $FGF1^{\triangle NT2}$ respectively are indicated as arrows **(B)** SEC-MALS analysis of the binding affinities of FGFR1c with ligands $FGF1^{WT}$, $FGF1^{\triangle HBS}$, $FGF1^{\triangle NT1}$, and $FGF1^{\triangle NT2}$ respectively in the presence of HS dodecasaccharide. The various FGF1 ligands were mixed with the FGFR1c ligand-binding domain (MW=25.4 kDa) and HS dodecasaccharide (MW=3 kDa) at a molar ratio of 1:1:1, and the mixtures were injected into TSK-Gel® SuperSW3000 GF column with phosphate buffered saline (pH 7.4). The 280 nm UV absorbance traces for the $FGF1^{WT}$-FGFR1c-HS, $FGF1^{\triangle NT1}$-FGFR1c-HS, $FGF1^{\triangle HBS}$-FGFR1c-HS, and $FGF1^{\triangle NT2}$-FGFR1c-HS complexes are colored red, green, blue and pink, respectively. A second line below each protein complex peak denotes the peak area selected for molecular weight calculation. **(C)** A Table showing the calculated and theoretical molecular mass of the different species analyzed as estimated from SEC-MALS analysis also showing a corresponding effect of dimerization stability on receptor binding abilities leading to varying mitogenic or metabolic effects, in accordance with our "threshold" model. **(D)** The SEC-MALS elution profiles of FGFR1c alone, $FGF1^{WT}$ alone, $FGF1^{\triangle NT2}$ alone and a mixture of $FGF1^{WT}$ with the FGFR1c ligand-binding domain and $FGF1^{\triangle NT2}$ with FGFR1c. Indicates that $FGF1^{WT}$ forms a stable complex with FGFR1c whereas the $FGF1^{\triangle NT2}$ is incapable of binding to FGFR1c ectodomain. **(E)** Dose-response for NIH 3T3 fibroblast proliferation to $FGF1^{WT}$, $FGF1^{\triangle NT1}$ and $FGF1^{\triangle HBS}$, respectively. Data from three independent measurements are presented as mean +/- SEM. *p<0.05, **p<0.01 vs PBS buffer control. **(F)** Immunoblots showing dose-dependent

activation of FGFR substrate 2a (FRS2α), and MAPK pathway (ERK1/2) by $FGF1^{WT}$, $FGF1^{\triangle NT1}$ and $FGF1^{\triangle HBS}$ in NIH 3T3 fibroblasts. **(G)** Cellular glucose uptake in response to stimulation of differentiated 3T3-L1 adipocytes by $FGF1^{WT}$, $FGF1^{\triangle NT1}$ and $FGF1^{\triangle HBS}$. Data from three independent measurements are presented as mean +/- SEM. ***p<0.001 vs vehicle control.

Supplemental Experimental Procedures

Protein Expression and Purification

The cDNA fragment encoding full-length wild-type human FGF1 ($FGF1^{WT}$, residues 1-155) was subcloned into the expression vector pET30a using the cloning sites NdeI and HindIII. The heparin binding mutant construct of FGF1 ($FGF1^{\triangle HBS}$) were achieved by sequentially introducing the Lys127Asp, Lys128Gln and Lys133Val into the $FGF1^{WT}$ expression construct using the QuikChange XL site-directed mutagenesis kit (Stratagene, La Jolla, CA). The wild-type and N-terminally truncated FGF1 (residues Lys25 to Asp155, $FGF1^{\triangle NT1}$; residues Lys29 to Asp155, $FGF1^{\triangle NT2}$) were expressed and purified as described previously The wild-type FGF1 was expressed and purified as described previously (Beenken et al., 2012). Competent BL21 (DE3) *Escherichia coli* cells were transformed with expression construct for $FGF1^{\triangle HBS}$, and were cultured at 37 °C to an A_{600} of 0.5 (Beckman DU530 UV-visible spectrometer) and induced with 1 mM isopropyl-L-thio-B-D-galactopyranoside (IPTG) for 4 h. The cells were then lysed using the Emulsiflex-C3 (Avestin, Inc., Ottawa, Canada) high volume homogenizer, and the soluble proteins were purified using cation exchange column (Source S, GE Healthcare, Piscataway, NJ) and size exclusion chromatography. The purity of all above proteins was estimated to be >98% based on SDS-PAGE analysis.

The DNA fragments encoding full-length, mature FGF8b (residues 23-215), full-length FGF8a (residues 34-215) were amplified by PCR and subcloned into the pET-30a bacterial expression vector. PCR was also used to generate the expression construct for the FGF8b Phe32Ala mutant ($FGF8b^{F32A}$). Each of the FGF8 isoforms and the FGFR ligand-binding regions (FGFR1c, residues A131-R365) were expressed in *Escherichia coli* as inclusion bodies as described previously (Olsen et al., 2006). Inclusion bodies were isolated and solubilized in 6 M guanidinium-hydrochloride, 20 mM EDTA, 20 mM DTT, and 50 mM Tris-HCl, pH 7.5. The solubilized proteins were dialyzed and purified as described previously (Beenken et al., 2012).

BaF3 cell line establishment

The murine pro-B BaF3 cell line is an IL3-dependent cell line that is completely devoid of endogenous FGFRs and Klotho coreceptors, and has no/negligible expression of HSPGs and hence does not respond to paracrine or endocrine FGF stimulation. However, upon forced expression of appropriate FGFRs and Klotho coreceptors and in the presence of exogenous HS this cell line can be made responsive to FGF. Accordingly, BaF3 cell line has served as an ideal vehicle for exploring FGF-FGFR specificity, cofactor/coreceptor requirement in FGF signaling in FGF biology. BaF3 cell line overexpressing FGFR1c wild type was generated as follows: BaF3 cells were infected with lentiviruses containing the FGFR1c gene. After 2 days' incubation in RPMI 1640 medium containing 0.3 mg/L L-glutamine, 10% fetal bovine serum (FBS), 50 nM beta-mercaptoethanol, 100 IU/mL penicillin, 100 mg/mL streptomycin sulfate, and 3 ng/mL murine IL-3 (R&D Systems, Minneapolis, MN) at 37 ℃/ 5% CO_2, the cells were selected for neomycin resistance to isolate the cell clones stably expressing

FGFR1c.

Cell Culture, Adipocyte Differentiation, Glucose Uptake

3T3-L1 preadipocytes, NIH 3T3 cells and rat hepatoma cell H4IIE (American Type Culture Collection, Manassas, VA) were cultured as described previously (Kharitonenkov et al., 2005; Kurosu et al., 2007). 3T3-L1 preadipocytes were seeded at a density of ~1500 cells/well in 100 µL culture medium in a 96-well plate and differentiated to mature adipocytes, and maintained for another 4 days prior to use. Glucose uptake was assayed using a Glucose Uptake Assay Kit (Abcam, Cambridge, MA). Briefly, 3T3-L1 adipocytes or H4IIE (5×10^4/well), which were cultured in 96-well plates, were serum-starved overnight, stimulated with indicated concentration of $FGF1^{WT}$ and its variants for 24 h, and then washed twice with KRPH buffer (15 mM HEPES, pH 7.4, 118 mM NaCl, 4.8 mM KCl, 1.2 mM $MgSO_4$, 1.3 mM $CaCl_2$, 1.2 mM KH_2PO_4, and 0.1% BSA), and 100 µL of KRPH buffer containing 2-Deoxyglucose (2-DG, 100µM) was added to each well. The control wells contained 100 µL of KRPH buffer without 2-DG (100 µM). The uptake reaction was performed at 37 °C for 1 h, terminated by the addition of 80µl extraction buffer. Then the standard procedures were followed according to the manufacturer's instructions. The amount of 2-DG in the test samples, which is proportional to the accumulated 2-DG-6-phosphate (2-DG6P), was calculated using the 2-DG6P plotted standard curve.

***In vivo* Protocol**

Male *db/db* (C57BLKS/J-*lepr^{db}/lepr^{db}*) and lean littermate control mice (*db/m*) were from the Model Animal Research Center of Nanjing University, China or Jackson Laboratory (Bar Harbor, Maine), and the protocols used in these studies were approved by the Animal Care and Use Committee of Wenzhou Medical University, China or the University of Louisville, USA. Animals were housed in a specific-pathogen-free animal facility with controlled environment (22±°C, 50-60% humidity, 12-hour light-dark cycle, lights on at 7 am) and free access to food and water. Before each study, the body weight was measured and the whole-blood glucose obtained from the mouse tail vein was measured using a FreeStyle complete blood glucose monitor (Abbott Diabetes Care Inc., Alameda, CA). The *db/db* mice were then randomized based on their glucose levels and body weights and placed into 3 groups: where these groups of mice were treated with $FGF1^{WT}$ or $FGF1^{\Delta HBS}$ and one group was treated with vehicle (PBS) served as the negative treatment control. In addition, the *db/m* mice were treated with PBS as model control.

For acute does-response and time-course study, blood samples were taken from conscious, fed animals by tail snip at the indicated time-points after a single intraperitoneal (IP) injection of $FGF1^{WT}$, $FGF1^{\Delta HBS}$ or vehicle. Blood glucose level was measured as described above. Before acute intraperitoneal glucose tolerance test (IPGTT) and intraperitoneal insulin tolerance test (IPITT), mice were fasted for 6 h starting from 8:00 am after a single injection (IP) of $FGF1^{WT}$ or $FGF1^{\Delta HBS}$ at 0.5 mg/kg body weight or vehicle. For IPGTT, mice were challenged with a glucose solution (2 g/kg body weight, IP), and their blood were collected at 0, 15, 30, 60 and 120 min post-injection, and the blood glucose levels were determined as described above and the plasma insulin levels were assayed using an Ultra-Sensitive Mouse Insulin ELISA Kit (Crystal Chem Inc., Downers Grove, IL) according to the manufacturer's instruction (Yong et al., 2011). For IPITT, mice were injected with human insulin (Humulin R, IP; Eli Lilly, Indianapolis, IN) at a dose of 2 unit/kg body weight. Blood glucose levels at 0, 15, 30, 60 and 120 min after insulin injection were measured as described above (Ize-Ludlow et al., 2011). Area under the curve (AUC) was calculated by the trapezoid rule for the glucose and insulin

tolerance curve using Origin 7.5 software (OriginLab Corporation, Northampton, MA).

For chronic efficacy evaluation, the mice were intraperitoneally injected with $FGF1^{WT}$, $FGF1^{\Delta HBS}$ at the dose of 0.5 mg/kg body weight or vehicle (PBS) every other day for four weeks or twelve weeks. At the indicated time-points, the blood glucose levels were determined as described above.

For high-fat diet feeding, male C57BL/6J mice were housed individually in Micro-Isolator cages and maintained from age of 3 weeks on high-fat diet (40 % fat; Harlan Teklad) with free access to water. After 12 weeks of either a standard diet or a high-fat diet feeding, mice were randomly assigned by body weight and fed blood glucose levels. The mice were subcutaneously injected with vehicle (PBS), $FGF1^{WT}$, or $FGF1^{\Delta HBS}$ (0.5mg/kg). Blood samples were taken from fed animals by tail snip at the indicated time-points after a single injection of $FGF1^{WT}$, $FGF1^{\Delta HBS}$ or vehicle and the blood glucose levels were assayed as described above.

The type 1 diabetic (T1D) model was induced in 5-week-old C57BL/6 mice by a single intraperitoneal injection of 150 mg/kg STZ in citrate buffer (pH4.5), while the control animals received the same volume of citrate buffer. After seven days, mice with blood glucose ≥300mg/dl (16.7mM) were considered as type 1 diabetics. Then, the STZ-induced T1D mice were intraperitoneally injected with $FGF1^{WT}$ or $FGF1^{\Delta HBS}$ for 3 months at a dose of 0.5 mg/kg every other day. Blood glucose levels and body weight were measured weekly. The plasma glucose levels were measured using a FreeStyle complete blood glucose monitor (Abbott Diabetes Care Inc., Alameda, CA)

Western Blot Analysis

The above cultured 3T3-L1 adipocytes, NIH-3T3 cells or H4IIE were starved for 12 h, stimulated with different dose of $FGF1^{WT}$ and $FGF1^{\triangle HBS}$ for 20 min, and then lysed for future use. The liver and adipose tissues of the male *db/db* and *db/m* mice were collected and lysed after 28-day treatment with or without $FGF1^{WT}$ and $FGF1^{\triangle HBS}$. Forty micrograms of lysate proteins from 3T3-L1 adipocytes, NIH 3T3, H4IIE cells or liver tissues were separated using 8-12% SDS-PAGE and electrotransferred onto a nitrocellulose membrane. The protein blots were probed with antibodies against phospho-FGFR1, FGFR1, phospho-ERK1/2, ERK1/2 (Cell Signaling Technology, Danvers, MA), FRS2α (Santa Cruz Biotechnology, Dallas, TX), phospho-FRS2α, Ki67, PCNA, SEREBP-1, FAS, SCD-1, β-actin and GAPDH (Abcam). The immunoreactive bands were then detected by incubating with the secondary antibody (Santa Cruz Biotechnology, Dallas, TX) conjugated with horseradish peroxidase and visualizing using enhanced chemiluminescence (ECL) reagents (Bio-Rad, Hercules, CA). The amount of the proteins were then analyzed using Image J analysis software version 1.38e (NIH, Bethesda, MD) and normalized against their respective controls.

RNA Extraction, cDNA Synthesis and Quantitative RT-PCR

Total RNA was extracted from Liver and adipose tissues with TRIzol reagent (Invitrogen, Carlsbad, CA). After quantified using a Nanodrop ND-1000 spectrophotometer, 1μg total RNA was used to synthesize first-strand complimentary DNA (cDNA) using reverse transcription kit (Promega, WI) following the manufacturer's instructions. Quantitative RT-PCR reactions were performed in duplicate on an ABI Prism 7500HT (PE Applied Biosystems) and were normalized to either GAPDH. All TaqMan® assay-on-demand primers were from Thermo Fisher Scientific Inc. (Grand Island, NY). Sequences were as follows: GAPDH, Mm99999915_g1; SREBF1, Mm00550338_m1; FAS, Mm00662319_m1; SCD-1, Mm00772290_m1.

Digestion of Lysate Proteins, HILIC Fractionation of Tryptic Digests and Enrichment of Phosphopeptides using TiO_2

3T3-L1 preadipocytes were lysed with a solution containing 9 M urea, 20 mM Tris, pH 8, 0.2 mM EDTA, and protease inhibitors (Complete tablet; Roche, Mannheim, Germany). Proteins were then reduced with DTT and alkylated with iodoacetamide prior to overnight digestion with trypsin at 37 °C. The tryptic peptides were desalted using StageTips and dried. The peptides were then fractionated using hydrophilic interaction liquid chromatography (HILIC) according to a previously published protocol (Zhang et al., 2014; Zhang and Neubert, 2011). All HILIC fractionations were performed on an Agilent 1100 HPLC system using a 1 × 250 mm TSKgel Amide-80 5 μm particle column (Tosoh Biosciences). Seventeen fractions were collected after HILIC separation. After drying by centrifuging under vacuum, peptides were reconstituted in 5% trifluoroacetic acid (TFA)/60% acetonitrile. Enrichment and cleanup were performed using TiO_2 beads (GL Sciences, Inc. Japan) in StageTips packed in house.

Liquid Chromatography-Mass Spectrometry (LC-MS)

For LC–MS, a Thermo Scientific EASY-nLC 1000 coupled to a Q Exactive mass spectrometer (Thermo Fisher Scientific) was used. A self-packed 75 μm × 20 cm reversed-phase column (Reprosil C18, 3 μm, Dr. Maisch GmbH, Germany) was used for peptide separation. The Q Exactive was operated in top 10 data-dependent mode with survey scans acquired at a resolution of 70 000 at *m*/*z* 200. MS/MS scans were set to a resolution of 17,500 at m/z 200. Spectra were acquired with a normalized collision energy of 27 eV and a dynamic exclusion duration of 30 s (Zhang et al., 2014; Zhang and Neubert, 2011).

Protein Identification and Quantitation

The raw files were processed using the MaxQuant computational proteomics platform (version 1.5.2.8) for peptide identification and quantitation. The fragmentation spectra were used to search the UniProt mouse protein database allowing up to two missed tryptic cleavages. Carbamidomethylation of cysteine was set as a fixed modification, and oxidation of methionine and protein N-terminal acetylation, D_4-lysine, $^{13}C_6$-arginine, $^{13}C_6$-$^{15}N_2$-lysine, and $^{13}C_6$-$^{15}N_4$-arginine were used as variable modifications for database searching. Both peptide and protein identifications were filtered at 1% false discovery rate (FDR).

Supplemental References

Beenken, A., Eliseenkova, A.V., Ibrahimi, O.A., Olsen, S.K., and Mohammadi, M. (2012). Plasticity in interactions of fibroblast growth factor 1 (FGF1) N terminus with FGF receptors underlies promiscuity of FGF1. J Biol Chem *287*, 3067-3078.

Ize-Ludlow, D., Lightfoot, Y.L., Parker, M., Xue, S., Wasserfall, C., Haller, M.J., Schatz, D., Becker, D.J., Atkinson, M.A., and Mathews, C.E. (2011). Progressive Erosion of beta-Cell Function Precedes the Onset of Hyperglycemia in the NOD Mouse Model of Type 1 Diabetes. Diabetes *60*, 2086-2091.

Kharitonenkov, A., Shiyanova, T.L., Koester, A., Ford, A.M., Micanovic, R., Galbreath, E.J., Sandusky, G.E., Hammond, L.J., Moyers, J.S., Owens, R.A*., et al.* (2005). FGF-21 as a novel metabolic regulator.

J Clin Invest *115*, 1627-1635.
Kurosu, H., Choi, M., Ogawa, Y., Dickson, A.S., Goetz, R., Eliseenkova, A.V., Mohammadi, M., Rosenblatt, K.P., Kliewer, S.A., and Kuro-o, M. (2007). Tissue-specific expression of betaKlotho and fibroblast growth factor (FGF) receptor isoforms determines metabolic activity of FGF19 and FGF21. J Biol Chem *282*, 26687-26695.
Olsen, S.K., Li, J.Y., Bromleigh, C., Eliseenkova, A.V., Ibrahimi, O.A., Lao, Z., Zhang, F., Linhardt, R.J., Joyner, A.L., and Mohammadi, M. (2006). Structural basis by which alternative splicing modulates the organizer activity of FGF8 in the brain. Genes Dev *20*, 185-198.
Yong, J., Rasooly, J., Dang, H., Lu, Y., Middleton, B., Zhang, Z., Hon, L., Namavari, M., Stout, D.B., Atkinson, M.A.*, et al.* (2011). Multimodality imaging of beta-cells in mouse models of type 1 and 2 diabetes. Diabetes *60*, 1383-1392.
Zhang, G., Bowling, H., Hom, N., Kirshenbaum, K., Klann, E., Chao, M.V., and Neubert, T.A. (2014). In-depth quantitative proteomic analysis of de novo protein synthesis induced by brain-derived neurotrophic factor. J Proteome Res *13*, 5707-5714.
Zhang, G., and Neubert, T.A. (2011). Comparison of three quantitative phosphoproteomic strategies to study receptor tyrosine kinase signaling. J Proteome Res *10*, 5454-5462.